NANO LETTERS

Observation of Giant Optical Linear Dichroism in a Zigzag Antiferromagnet FePS₃

Qi Zhang,*,[¶] Kyle Hwangbo,[¶] Chong Wang, Qianni Jiang, Jiun-Haw Chu, Haidan Wen, Di Xiao, and Xiaodong Xu*

Read Online

ACCESS | Metrics & More | Article Recommendations | Supporting Information

ABSTRACT: Direct optical probing of the antiferromagnetic order parameter in atomically thin samples is challenging, for example, via magneto-optical spectroscopy, due to the lack of net magnetization. Here, we report zigzag-antiferromagnetism (AFM) induced optical linear dichroism (LD) in layered transition-metal thiophosphate FePS₃ down to the monolayer limit. The observed LD is giant despite having the optical wave vector parallel to the Néel vector. The LD is at least one order of magnitude larger than those reported in other antiferromagnetic systems, where the optical wave vector is orthogonal to the Néel vector. The large LD enables the probe of 60° orientated zigzag-AFM domains. The optical anisotropy in FePS₃ originates from an electronic anisotropy associated with the zigzag direction of the AFM order and is independent of the spin-pointing direction. Our findings point to a new optical approach for the investigation and control of zigzag or stripe magnetic order in strongly correlated systems.

KEYWORDS: 2D materials, 2D magnet, antiferromagnet, iron phosphorus trisulfide
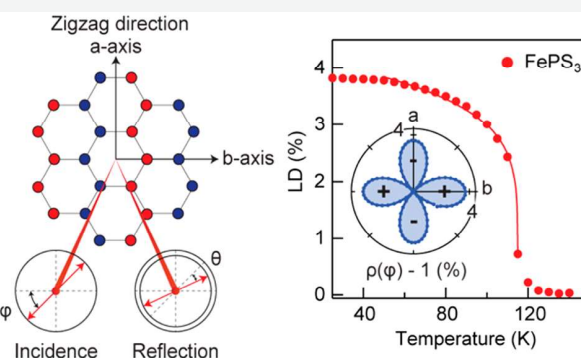
Two-dimensional honeycomb lattice can exhibit a number of magnetic ground states. Depending on the relative strength of the first, second, and third nearest neighbor exchange interaction (J_1, J_2, and J_3, respectively), different magnetic phases, such as ferromagnetism (FM), zigzag-antiferromagnetism (AFM), stripe-AFM, and Néel-AFM, can form.[1,2] While in noncolinear spin alignment systems, spiral AFM order[3] or Kitaev-type quantum spin liquid phase may appear.[4] Among the various van der Waals (vdW) magnets, transition-metal thiophosphates, XPS_3 (X = Fe, Ni, and Mn), form a unique class of 2D antiferromagnets with intralayer antiferromagnetic order on a honeycomb spin−lattice.[5] FePS₃ and NiPS₃ are zigzag-antiferromagnets, while their isostructural compound MnPS₃ is a Néel-antiferromagnet,[6−9] as illustrated in Figures.1a and b. In addition to 2D antiferromagnetism, previous studies of XPS_3 have uncovered strongly coupled spin and charge orders,[10] highly anisotropic excitons,[11−13] and strong electron correlation[14] in the family. Hence, this class of vdW antiferromagnets offers a desirable testing ground for 2D magnetism and also provides new opportunities of exploring its interplay with other correlated order parameters at the 2D limit.

Experimental detection of an antiferromagnetic order in atomically thin films is challenging. While the time-reversal symmetry is broken in antiferromagnets, many colinear AFM systems sustain a combined time-reversal and inversion symmetry, which results in a vanishing magneto-optical (MO) effect to the first order of the local magnetic moment, M. To overcome this difficulty, the Voigt effect (or the Cotton-Mouton effect), which is proportional to $|M|^2$, has been used to detect AFM phases by monitoring the magnetic linear dichroism (LD) or birefringence (LB), especially with X-ray light.[15] When the X-ray light is in resonance with the inner shell $p−d$ transitions of magnetic transition metal atoms, antiferromagnets exhibit an anisotropic X-ray absorption along ($I_∥$) and across ($I_⊥$), the direction of the Néel vector, which is known as X-ray magnetic linear dichroism (XMLD). The linear dichroism, defined as $LD = \frac{I_∥ - I_⊥}{I_∥ + I_⊥}$, typically ranges from 1 to 10%.[16,17] While XMLD is a powerful technique to probe antiferromagnetic order, it usually requires access to sophisticated synchrotron facilities.

In the optical frequency range, the magnetic LD and LB originating from the Voigt effect are orders of magnitude weaker than their X-ray counterparts. Thus, the direct
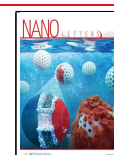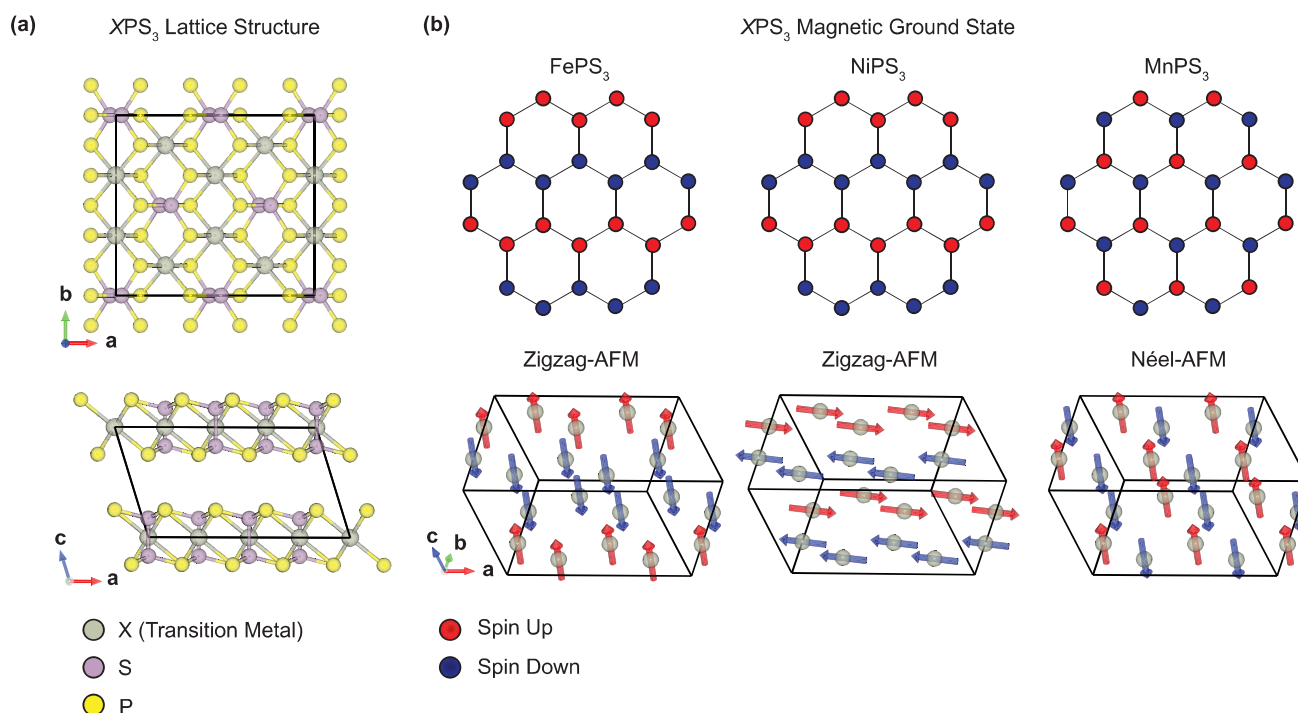
Figure 1. Lattice and spin structure of the XPS_3 (X = Fe, Ni, Mn). (a) Lattice structure: The transition metal atoms form a honeycomb lattice surrounded by sulfur atoms. Bulk XPS_3 has a monoclinic structure, where the shift between layers is along the a-axis. (b) Spin structure: $FePS_3$ and $NiPS_3$ have zigzag-AFM order below T_N. The nearby zigzag lines have opposite spin orientation (indicated by red and blue dots), while $MnPS_3$ is Néel-AFM. For both $FePS_3$ and $NiPS_3$, the zigzag direction is along the crystal a-axis. The structures were drawn using VESTA.[35]

Table 1. Summary of Reported LD and LB in AFMs

	materials	ground state	LD (%)	Θ (mrad)	T_N (K)	wavelength (nm)	thickness
XPS_3 (this work)	$FePS_3$	zigzag AFM	1.18%	6	117	633	1.4 nm (2L)
	$NiPS_3$	zigzag AFM	2%	10	154	633	4 nm (~5L)
iron pnictides and related systems	$BaFeCoAs$[22]	AFM, nematic		0.2	48.66	400	bulk
	$Fe_{1/3}NbS_2$[31]	AFM, nematic		1	43	633	bulk
	Fe_2As[32]	AFM		0.5	350	783	80 nm
	$FeBO_3$[33]	ferrimagnet/AFM	6%[a]		348		bulk
	MnF_2[20]	AFM	1%[a]		67		bulk (>0.1 mm)
	$GaMnAs$[34]	FM		0.6	50	815	350 nm
	$CuMnAs$[18]	AFM		0.1	465	800	10 nm
XMLD	NiO[17]	AFM	~10%		525	Xray	20 ML
	Fe_2O_3[16]	AFM	~10%			Xray	10 nm

[a]LD listed is for some sharp exciton lines, otherwise LD is much weaker.

measurement of 2D antiferromagnetic order, in this way, is difficult.[18] For bulk crystals, these effects have been previously observed in transition metal fluorides (i.e., FeF_2, MnF_2, CoF_2, etc.)[19−21] and iron pnictides. In transition metal fluorides, the formation of antiferromagnetic ground states slightly modifies the existing bulk optical birefringence. For the iron pnictides, a material family that hosts unconventional superconductivity, both the stripe antiferromagnetic order and the nematic order have been shown to induce LD and LB.[22] The polarization rotation θ of linearly polarized incident light has been shown to range from 0.1 to 1 mrad for bulk materials, as listed in Table 1. However, for a nanometer thick thin film, this effect is expected to be negligible due to the short propagation length.

In this work, we observe giant optical linear dichroism in $FePS_3$ thin films down to the monolayer limit, associated with the zigzag-AFM order. The observed LD and linear polarization rotation are on the order of 1% and 10 mrad in θ,

respectively, and comparable with the XMLD values in the resonance condition. Distinct from LD that stems from the Voigt effect, the giant LD in $FePS_3$ originates from an electronic anisotropy associated with the direction of zigzag spin chains in the AFM ground state. These findings open new venues for the optical detection and control of zigzag or stripe magnetic order in the 2D limit.

$FePS_3$ flakes were prepared by mechanical exfoliation of bulk crystals on SiO_2/Si substrates. We first measure the sample reflectivity with a linearly polarized, normally incident 1.96 eV laser at 7 K (Figure 2a). Experimental setup is shown in Figure S1. As illustrated in Figure 2b, the normalized intensity of the reflected light (ρ) varies as the polarization angle (φ) of the incident light is rotated with respect to the crystal b-axis for $FePS_3$. The reflectivity has a 2-fold rotational symmetry, where the reflectivity is high when the light is linearly polarized along the b-axis of the crystal and low when the light is polarized
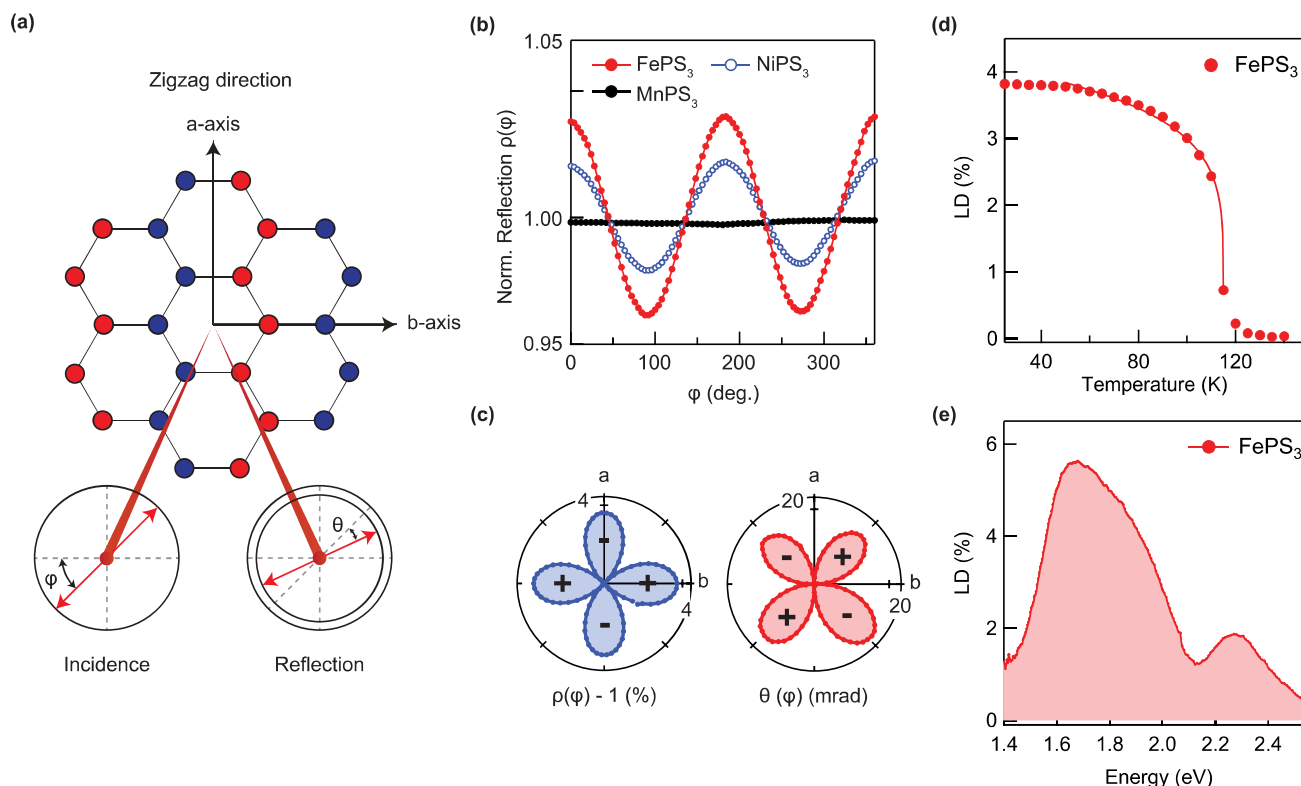
Figure 2. |Optical linear dichroism induced by zigzag-AFM order. (a) Schematic of the linear dichroism measurements. Linearly polarized light is normally incident on the XPS_3 hexagonal plane. The angle between the linear polarization and crystal b-axis is φ. Because of the anisotropic absorption/reflection along and across the zigzag direction, the reflected light has a polarization rotation θ and φ-dependent intensity. (b) Normalized reflection intensity $\rho(\varphi)$ for 1.96 eV excitation. Prominent anisotropic reflection was observed in both zigzag-AFM $FePS_3$ and $NiPS_3$ flakes, but not in the Néel-type $MnPS_3$. (c) Normalized intensity anisotropy $\rho(\varphi) - 1$ and polarization rotation $\theta(\varphi)$ at 1.96 eV for $FePS_3$. (d) Linear dichroism (LD) as a function of temperature. LD disappears above the Néel temperature 117 K. Solid line is a guide to the eye. (e) LD spectrum for a 10 nm (~14 layers) $FePS_3$ flake exfoliated on a sapphire substrate measured at 7K.

along the a-axis. The correlation between the zigzag spin alignment direction and the crystal axes was established through X-ray scattering measurements (Figure S6) and subsequent optical reflection measurements. The relationship was further confirmed by polarization-resolved Raman spectroscopy measurements (see Figures S2 and S3 for further details) and first-principle calculations (Figure 3c,d). Previous neutron scattering measurements have determined the zigzag spin chain to be parallel to the a-axis of the crystal.[6,23]

The normalized reflection is defined as $\rho(\varphi) = \frac{2R(\varphi)}{(R_\parallel + R_\perp)} = \frac{2}{(R_\parallel + R_\perp)}(R_\parallel \cos^2(\varphi) + R_\perp \sin^2(\varphi))$, where $R(\varphi)$ is the measured reflected light intensity at the polarization angle φ. $R_\parallel$ ($R_\perp$) is for the polarization along (across) the zigzag direction. Since LD is defined as $\frac{R_\parallel - R_\perp}{R_\parallel + R_\perp}$, we obtain $\rho(\varphi) - 1 = LD \times \cos(2\varphi)$, which can be measured directly with high precision via polarization modulation spectroscopy (see Methods). Figure 2c shows a direct measurement of $\rho(\varphi) - 1$. The direction of the negative lobes is along the zigzag alignment. For a 10 nm thick flake, LD reaches about 4%.

The observed LD can be naturally attributed to the zigzag antiferromagnetism, which breaks the three-fold rotational symmetry. To support this interpretation, we also perform LD measurements on $NiPS_3$ (blue circles in Figure 2b), which shows the same anisotropic response as $FePS_3$. In contrast, the

Néel-antiferromagnet $MnPS_3$ exhibits an isotropic optical response under the same experimental condition. Though all three XPS_3 compounds have a monoclinic structure with $C2/m$ symmetry above and below the Néel temperature, we only observe LD in $NiPS_3$ and $FePS_3$, both of which possess a zigzag antiferromagnetic ground state, with LD having a precise directional correlation to the zigzag axis. Furthermore, we measure the temperature dependence of the linear dichroism in $FePS_3$. As shown in Figure 2d, LD in $FePS_3$ exhibits a strong dependence on temperature, disappearing above the Néel temperature (~117 K). The combination of all these results demonstrates a magnetic origin of the observed optical anisotropy.

Along with the LD, the zigzag-AFM also induces a polarization rotation θ, as shown in Figure 2c, where $\theta(\varphi) = \theta_0 \sin(2\varphi)$ and $\theta_0 \approx LD/2$. Interestingly, the observed ρ and θ_0 in $FePS_3$ are giant, reaching 1% or 10 mrad even at the few-layer limit. This is at least one order of magnitude larger than the values reported previously in other AFM systems in 3D bulk crystals, and even comparable to those observed through resonant XMLD, as summarized in Table 1. We further study LD as a function of photon energy. As shown in Figure 2e, two LD peaks were found at around 1.8 and 2.4 eV, both of which have been assigned to multiple $d-d$ transitions in a previous study.[24] As expected, the two peaks disappear above the Néel temperature (Figure S4).
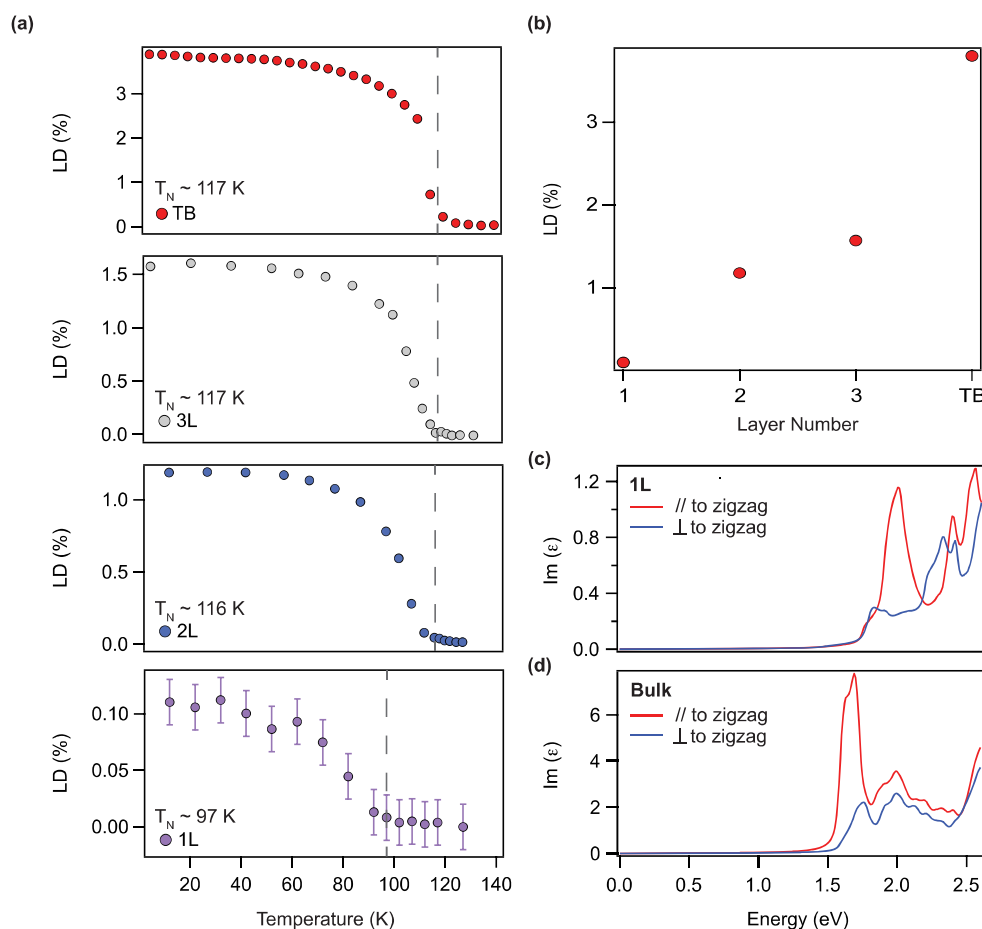
Figure 3. Temperature-dependent linear dichroism measurements for different thicknesses of $FePS_3$. (a) Temperature-dependent linear dichroism signal of thin bulk (TB), 3L, 2L, and 1L $FePS_3$. The dashed lines indicate the Néel temperatures. Error bars, where visible, represent the estimated noise associated with the experimental setup. (b) Extracted values of LD versus the layer number for $FePS_3$ at base temperature (7 K). (c) Theoretical calculation of the imaginary part of the dielectric constant for an undistorted monolayer $FePS_3$ along (red curve) and across (blue curve) the zigzag spin alignment direction. (d) Theoretical calculation of the imaginary part of the dielectric constant for undistorted bulk $FePS_3$.

The strong optical anisotropy remains in atomically thin flakes, persisting down to a monolayer. We identify the sample thicknesses through a combination of atomic force microscopy and optical contrast. Figure 3a shows the temperature-dependent LD measurements for various thicknesses of $FePS_3$. The Néel temperature shifts to lower temperatures as the layer number is reduced, which is consistent with thickness-dependent T_c-shift that has been observed in other vdW magnets.[25,26] LD signal drops sharply as the flakes are thinned down from bilayer to monolayer but remains appreciable at the monolayer limit (Figure 3a,b). These findings agree with previous reports of persistent magnetic order down to monolayer in $FePS_3$ using Raman spectroscopy,[27,28] further corroborating the relationship between the magnetic order and the LD signal. In addition to the shift in the transition temperature, there is a correspondingly large drop in LD going from 2L-to-1L. Although the interlayer coupling is weak in bulk and multilayer van der Waals magnets, they are still considered quasi-2D magnetic systems. We speculate that the large change in LD is a result of transitioning from a quasi-2D magnetic system to a truly two-dimensional spin system. In this sense, the change from 2L-to-1L is qualitatively different from 3L-to-2L. Strong spin fluctuation and absence of interlayer exchange coupling will weaken the

long-range spin order in the monolayer limit. Similar effects have been reported in other monolayer vdWs magnets, for example, $Cr_2Ge_2Te_6$ and CrI_3.[25,29] We note that further theoretical efforts and experiments are required to fully understand this observation.

As discussed earlier, the zigzag antiferromagnetic phase of $FePS_3$ retains combined time reversal and spatial inversion symmetry, which prevents a linear magneto-optical response. Hence, despite the strength of the observed LD signal, we rule out first-order magneto-optical effects as the source of the linear dichroism. Symmetry considerations point toward linear dichroism to be proportional to the square of the local magnetic moment, $|M|^2$. Although the Voigt effect has the same $|M|^2$ dependence, it is typically observed in systems with spin alignments that are perpendicular to the light wave vector. In $FePS_3$, the spin is Ising-like and parallel to the light propagation direction, and the in-plane magnetic susceptibility anisotropy is small. Thus, the observed strong LD in the zigzag-AFM phase is associated with the symmetry breaking by the formation of zigzag chains, instead of the spin pointing direction (Voigt effect).

A first-order in-plane lattice distortion (around 0.2%) occurs along with the zigzag-AFM phase transition in $FePS_3$.[30] The distorted honeycomb lattice could, in principle, lead to an
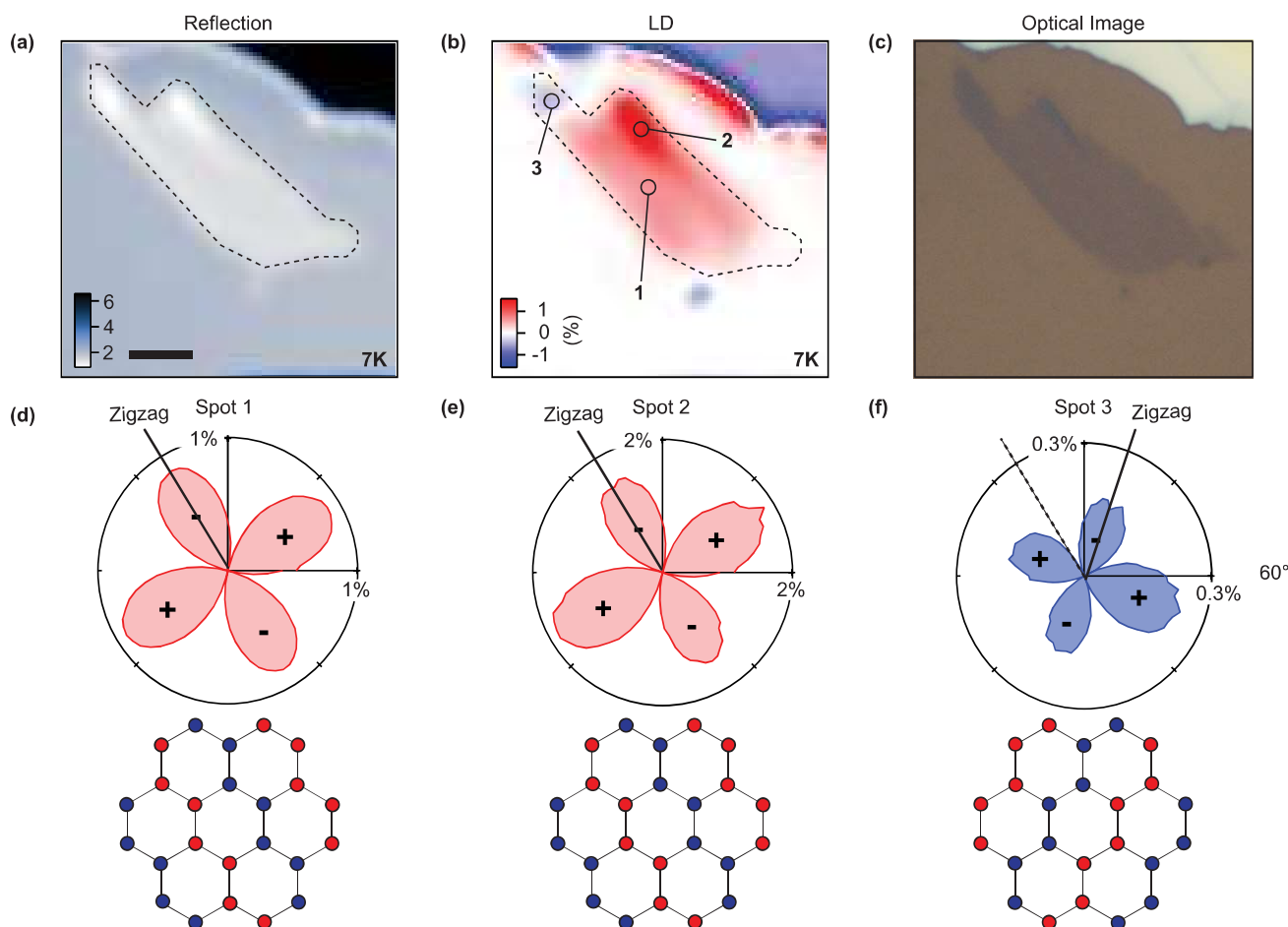
Figure 4. Zigzag AFM domains revealed by spatially resolved linear dichroism map. (a) Reflection, (b) LD, and (c) microscope image of a FePS$_3$ flake at 1.96 eV. Scale bar: 5 μm. In (b), spot 1 is a 3L area, while spots 2 and 3 are from two small 6L and 5L area on the same flake. (d−f) Angular dependence of ρ (φ) −1 for spots 1−3 respectively (top) as well as their corresponding schematics of spin configuration (bottom). The zigzag orientation in the 5L area (spot 3) is 60° off the main 3L zigzag direction. Data are taken at 7 K.

anisotropy in the electronic structure along and across the zigzag direction and contribute to the optical LD. In contrast, there are no reports of such in-plane lattice distortion in NiPS$_3$. The similarity in LD magnitude between the two materials, despite the lack of lattice distortion in NiPS$_3$, suggests that zigzag-AFM is indeed the main contributing element to the observed optical anisotropy.

Our theoretical analysis further supports the magnetic origin of the giant optical LD in FePS$_3$. We performed a first-principles band structure calculation to derive the imaginary part of the dielectric constant (further details on the calculations can be found in the Methods section). Calculations show that a nonmagnetic and undistorted monolayer FePS$_3$ has no optical anisotropy, as expected of a system with no broken rotational symmetry. Only when zigzag antiferromagnetism is introduced do we see a pronounced difference in the permittivity along and across the zigzag directions for both monolayer and bulk with undistorted lattices (Figure 3c,d). The formation of zigzag spin chains induces an anisotropy in electronic band structures as hopping along the zigzag axis is energetically preferred over hopping orthogonally across the spin chains since the former option does not require a spin flip. The electronic anisotropy that arises from the zigzag-AFM order is independent of the spin

pointing direction. Anisotropic band structures lead to anisotropic optical response. The observed LD in the visible range is mainly associated with the transitions within Fe d-orbitals

Using the uncovered connection between LD and zigzag antiferromagnetism, we can optically probe zigzag-AFM domains. Figure 4a shows the reflection raster image of a 3L FePS$_3$ flake with a small 5L area on the top left corner. The corresponding LD image is shown in Figure 4b. The 3L region has opposite sign of LD compared to the 5L area, indicating the existence of AFM domains. The drop in LD for the 5L suggests an existence of vertical domains. To determine the zigzag domain orientation, we performed angular dependence of differential LD signals (i.e., $\rho(\varphi) - 1$) at selected positions on the 3L (spots 1 and 2, Figure 4d,e) and the 5L (spot 3, Figure 4f). The negative lobes indicate the low optical reflection direction, corresponding to the zigzag alignment direction. The data clearly show that the zigzag-AFM direction of the 3L is rotated 60-degrees with respect to the 5L zigzag direction. This result indicates that, for this type of honeycomb antiferromagnets, it is possible to engineer three magnetic domains along the three possible zigzag directions. We note that, for most thin flakes with homogeneous thicknesses, there was only a single magnetic domain of zigzag spin chain

direction, which was robust under thermal cycles since the zigzag spin chain is pinned along the monoclinic stacking direction of the crystal.

Overall, the results above establish a prominent connection between linear dichroism and zigzag-AFM order in $FePS_3$. This connection not only offers an effective static probe of AFM, for example, zigzag domain imaging, but also may enable ultrafast optical measurement of AFM dynamics and its critical behaviors. These findings pave the way for implementing optical control of the coupled magnetic, electronic, and lattice degrees of freedom in strongly correlated 2D materials.

Methods. *Sample Fabrication.* Single crystals of $FePS_3$ were synthesized by chemical vapor transport (CVT) method using iodineas the transport agent. Stoichiometric amounts of iron powder (99.998%), phosphorus powder (98.9%), and sulfur pieces (99.9995%) were mixed with iodine (1 mg/cm^3) and sealed in quartz tubes (10 cm in length) under high vacuum. The tubes were placed in a horizontal one-zone tube furnace with the charge near the center of the furnace. Sizeable crystals ($10.0 \times 10.0 \times 0.5$ mm^3) were obtained after gradually heating the precursor up to 750 °C, dwelling for a week and cooling down to room temperature. Single crystals of $MnPS_3$ were synthesized with the same growth condition, while single crystals of $NiPS_3$ were synthesized in a similar growth process but with the maximum temperature up to 950 °C instead of 750 °C.

The crystals were exfoliated onto (90 nm) SiO_2/Si substrate in an argon gas protected glovebox. The layer thicknesses were identified through a combination of atomic force microscopy in the glovebox and optical contrast analysis. To protect the samples from degrading in ambient conditions during sample transport prior to loading into the cryostat, the samples were sealed in a copper sample holder with a transparent coverslip inside the glovebox. The total time the sealed samples spent outside of the glovebox before loading was less than 10 min.

Optical Measurements. For all low-temperature optical measurements, samples were measured in a closed-cycle cryostat (7 to 300 K) in high-vacuum.

Polarization Modulation Spectroscopy for Detecting Linear Dichroism. The measurements were carried out in a reflection geometry. A 633 nm (1.96 eV) HeNe laser was double-modulated by a photoelastic modulator (PEM) with a maximum retardance of $\lambda/2$ and a mechanical chopper. Upon phase modulation, the light was passed through a halfwave waveplate and then was focused down onto the sample at a normal incidence with an objective lens. A laser power of 4 μW was used to minimize sample heating. The reflected beam was received by a photodiode and further demodulated at 100 kHz and 1 kHz, which corresponds to the PEM linear polarization modulation, and the chopper modulation, respectively. By rotating the halfwave waveplate, $\rho(\varphi) - 1$ and LD can be measured. For detecting polarization rotation angle θ, a polarizer was placed in front of the photodiode. The optical setup is illustrated in Figure S1.

Linear Dichroism Spectrum. In a setup similar to linear dichroism, a supercontinuum laser with a tunable filter set was utilized for the linear dichroism spectrum. Wavelength tuning was achieved by scanning the filter along with the PEM retardance. Broadband polarizer, beamsplitter, and halfwave plate were used.

DFT Calculations. Our DFT calculations are performed with the Vienna Ab initio Simulation Package (PRB 54 11169, PRB 59 1758). The projector augmented wave potential (PRB 50 17953) and Perdew—Burke—Ernzerhof functional (PRL 77 3865) are utilized to describe the electron—ion and electron—electron interactions, respectively. For DFT calculations, the Brillouin zone is sampled with a $12 \times 8 \times 8$ mesh and the plane wave energy cutoff is set to 267.882 eV. A Hubbard U of 3 eV is added to account for the strong electron—electron repulsion on the iron atoms. Experimental lattice constants are used, and the internal atom positions are relaxed until the force on each atom are smaller than 0.001 eV/Angstrom. For monolayer calculations, the atomic structure is cut from the bulk and then symmetrized to have a D3d point group. No atomic relaxation is performed for the monolayer structure. The wannier90 package (JPCM 32 165902) is utilized to construct a tight binding Hamiltonian, which is then used to compute linear dichroism with a $160 \times 80 \times 80$ mesh in the Brillouin zone.

■ ASSOCIATED CONTENT

Ⓢ Supporting Information

The Supporting Information is available free of charge at https://pubs.acs.org/doi/10.1021/acs.nanolett.1c02188.

Schematic diagram for LD setup, Raman scattering characterization of $FePS_3$, determining zigzag AFM direction of LD, wavelength dependence of LD in $FePS_3$ for select temperatures, theoretical calculation of LD spectrum for 2 nm $FePS_3$ flake on sapphire substrate, X-ray scattering measurements of bulk $FePS_3$ (PDF)

■ AUTHOR INFORMATION

Corresponding Authors

Qi Zhang — *Department of Physics, University of Washington, Seattle, Washington 98195, United States; Advanced Photon Source, Argonne National Laboratory, Lemont, Illinois 60439, United States;* Email: zhangqi@nju.edu.cn

Xiaodong Xu — *Department of Physics and Department of Materials Science and Engineering, University of Washington, Seattle, Washington 98195, United States;* ⓞ orcid.org/0000-0003-0348-2095; Email: xuxd@uw.edu

Authors

Kyle Hwangbo — *Department of Physics, University of Washington, Seattle, Washington 98195, United States;* ⓞ orcid.org/0000-0001-8099-7506

Chong Wang — *Department of Physics, Carnegie Mellon University, Pittsburgh, Pennsylvania 15213, United States*

Qianni Jiang — *Department of Physics, University of Washington, Seattle, Washington 98195, United States*

Jiun-Haw Chu — *Department of Physics, University of Washington, Seattle, Washington 98195, United States*

Haidan Wen — *Advanced Photon Source, Argonne National Laboratory, Lemont, Illinois 60439, United States*

Di Xiao — *Department of Physics, Carnegie Mellon University, Pittsburgh, Pennsylvania 15213, United States*

Complete contact information is available at:
https://pubs.acs.org/10.1021/acs.nanolett.1c02188

Author Contributions

[¶]These authors contributed equally to this work. QZ and XX conceived the experiment. QZ and KH fabricated the samples and performed the optical measurements. CW and DX calculated the optical anisotropy. QZ, KH, XX, HW, JH, and DX analyzed and interpreted the results. QJ synthesized the

crystals. KH, QZ, and XX wrote the paper with input from all authors. All authors discussed the results.

Notes

■ ACKNOWLEDGMENTS

■ REFERENCES

(1) Li, P. H. Y.; Bishop, R. F.; Farnell, D. J. J.; Campbell, C. E. Phase diagram of a frustrated Heisenberg antiferromagnet on the honeycomb lattice: The J1-J2-J3 model. *Phys. Rev. B: Condens. Matter Mater. Phys.* **2012**, *86* (14), 144404 DOI: 10.1103/PhysRevB.86.144404.

(2) Sivadas, N.; Daniels, M. W.; Swendsen, R. H.; Okamoto, S.; Xiao, D. Magnetic ground state of semiconducting transition-metal trichalcogenide monolayers. *Phys. Rev. B: Condens. Matter Mater. Phys.* **2015**, *91* (23), 235425 DOI: 10.1103/PhysRevB.91.235425.

(3) Reuther, J.; Thomale, R.; Rachel, S. Spiral order in the honeycomb iridate Li2IrO3. *Phys. Rev. B: Condens. Matter Mater. Phys.* **2014**, *90* (10), 100405 DOI: 10.1103/PhysRevB.90.100405.

(4) Kitaev, A. Anyons in an exactly solved model and beyond. *Ann. Phys.* **2006**, *321* (1), 2−111.

(5) Le Flem, G.; Brec, R.; Ouvard, G.; Louisy, A.; Segransan, P. Magnetic interactions in the layer compounds MPX3 (M = Mn, Fe, Ni; X = S, Se). *J. Phys. Chem. Solids* **1982**, *43* (5), 455−461.

(6) Kurosawa, K.; Saito, S.; Yamaguchi, Y. Neutron Diffraction Study on MnPS3 and FePS3. *J. Phys. Soc. Jpn.* **1983**, *52* (11), 3919−3926.

(7) Brec, R. Review on structural and chemical properties of transition metal phosphorous trisulfides MPS3. *Solid State Ionics* **1986**, *22* (1), 3−30.

(8) Balkanski, M.; Jouanne, M.; Scagliotti, M. Magnetic ordering induced Raman scattering in FePS3 and NiPS3 layered compounds. *Pure Appl. Chem.* **1987**, *59* (10), 1247−1252.

(9) Wildes, A. R.; Simonet, V.; Ressouche, E.; Mcintyre, G. J.; Avdeev, M.; Suard, E.; Kimber, S. A. J.; Lançon, D.; Pepe, G.; Moubaraki, B.; Hicks, T. J. Magnetic structure of the quasi-two-dimensional antiferromagnet NiPS3. *Phys. Rev. B: Condens. Matter Mater. Phys.* **2015**, *92* (22), 224408 DOI: 10.1103/PhysRevB.92.224408.

(10) Kim, S. Y.; Kim, T. Y.; Sandilands, L. J.; Sinn, S.; Lee, M.-C.; Son, J.; Lee, S.; Choi, K.-Y.; Kim, W.; Park, B.-G.; Jeon, C.; Kim, H.-D.; Park, C.-H.; Park, J.-G.; Moon, S. J.; Noh, T. W. Charge-Spin Correlation in van der Waals Antiferromagnet NiPS3. *Phys. Rev. Lett.* **2018**, *120* (13), 136402 DOI: 10.1103/PhysRevLett.120.136402.

(11) Hwangbo, K.; Zhang, Q.; Jiang, Q.; Wang, Y.; Fonseca, J.; Wang, C.; Diederich, G. M.; Gamelin, D. R.; Xiao, D.; Chu, J.-H.; et al. Highly anisotropic excitons and multiple phonon bound states in a van der Waals antiferromagnetic insulator. *Nat. Nanotechnol.* **2021**, *16*, 1−6.

(12) Kang, S.; Kim, K.; Kim, B. H.; Kim, J.; Sim, K. I.; Lee, J.-U.; Lee, S.; Park, K.; Yun, S.; Kim, T.; et al. Coherent many-body exciton in van der Waals antiferromagnet NiPS3. *Nature* **2020**, *583* (7818), 785−789.

(13) Wang, X.; Cao, J.; Lu, Z.; Cohen, A.; Kitadai, H.; Li, T.; Tan, Q.; Wilson, M.; Lui, C. H.; Smirnov, D.; Sharifzadeh, S.; Ling, X. Spin-induced linear polarization of photoluminescence in antiferromagnetic van der Waals crystals. *Nat. Mater.* **2021**, *20*, 964.

(14) Wang, Y.; Ying, J.; Zhou, Z.; Sun, J.; Wen, T.; Zhou, Y.; Li, N.; Zhang, Q.; Han, F.; Xiao, Y.; Chow, P.; Yang, W.; Struzhkin, V. V.; Zhao, Y.; Mao, H.-K. Emergent superconductivity in an iron-based honeycomb lattice initiated by pressure-driven spin-crossover. *Nat. Commun.* **2018**, *9* (1), 1914 DOI: 10.1038/s41467-018-04326-1.

(15) Mertins, H.-C.; Oppeneer, P. M.; Kuneš, J.; Gaupp, A.; Abramsohn, D.; Schäfers, F. Observation of the X-Ray Magneto-Optical Voigt Effect. *Phys. Rev. Lett.* **2001**, *87* (4), 47401 DOI: 10.1103/PhysRevLett.87.047401.

(16) Kuiper, P.; Searle, B. G.; Rudolf, P.; Tjeng, L. H.; Chen, C. T. X-ray magnetic dichroism of antiferromagnet Fe2O3: The orientation of magnetic moments observed by Fe 2p x-ray absorption spectroscopy. *Phys. Rev. Lett.* **1993**, *70* (10), 1549−1552.

(17) Alders, D.; Vogei, J.; Levelut, C.; Peacor, S.; Hibma, T.; Sacchi, M.; Tjeng, L.; Chen, C.; Van der Laan, G.; Thole, B.; et al. Magnetic x-ray dichroism study of the nearest-neighbor spin-spin correlation function and long-range magnetic order parameter in antiferromagnetic NiO. *EPL (Europhysics Letters)* **1995**, *32* (3), 259.

(18) Saidl, V.; Nemec, P.; Wadley, P.; Hills, V.; Campion, R. P.; Novák, V.; Edmonds, K. W.; Maccherozzi, F.; Dhesi, S. S.; Gallagher, B. L.; Trojánek, F.; Kuneš, J.; Železný, J.; Malý, P.; Jungwirth, T. Optical determination of the Néel vector in a CuMnAs thin-film antiferromagnet. *Nat. Photonics* **2017**, *11* (2), 91−96.

(19) Jahn, I. R.; Dachs, H. Change of the optical birefringence associated with the antiferromagnetic ordering of MnF2, FeF2, CoF2, and NiF2. *Solid State Commun.* **1971**, *9* (18), 1617−1620.

(20) Kharchenko, N.; Miloslavskaya, O.; Milner, A. Magnetic linear dichroism of an antiferromagnetic MnF 2 crystal: Oddness in two different antiferromagnetic states. *Bull. Russ. Acad. Sci.: Phys.* **2007**, *71* (11), 1536−1538.

(21) Belanger, D. P.; King, A. R.; Jaccarino, V. Temperature dependence of the optical birefringence of MnF2, MgF2, and ZnF2. *Phys. Rev. B: Condens. Matter Mater. Phys.* **1984**, *29* (5), 2636−2643.

(22) Patz, A.; Li, T.; Ran, S.; Fernandes, R. M.; Schmalian, J.; Bud'Ko, S. L.; Canfield, P. C.; Perakis, I. E.; Wang, J. Ultrafast observation of critical nematic fluctuations and giant magnetoelastic coupling in iron pnictides. *Nat. Commun.* **2014**, *5* (1), 3229 DOI: 10.1038/ncomms4229.

(23) Lançon, D.; Walker, H. C.; Ressouche, E.; Ouladdiaf, B.; Rule, K. C.; Mcintyre, G. J.; Hicks, T. J.; Rønnow, H. M.; Wildes, A. R. Magnetic structure and magnon dynamics of the quasi-two-dimensional antiferromagnet FePS3. *Phys. Rev. B: Condens. Matter Mater. Phys.* **2016**, *94* (21), 214407 DOI: 10.1103/PhysRevB.94.214407.

(24) Joy, P. A.; Vasudevan, S. Optical-absorption spectra of the layered transition-metal thiophosphates MPS3 (M = Mn, Fe, and Ni). *Phys. Rev. B: Condens. Matter Mater. Phys.* **1992**, *46* (9), 5134−5141.

(25) Huang, B.; Clark, G.; Navarro-Moratalla, E.; Klein, D. R.; Cheng, R.; Seyler, K. L.; Zhong, D.; Schmidgall, E.; Mcguire, M. A.; Cobden, D. H.; Yao, W.; Xiao, D.; Jarillo-Herrero, P.; Xu, X. Layer-dependent ferromagnetism in a van der Waals crystal down to the monolayer limit. *Nature* **2017**, *546* (7657), 270−273.

(26) Fei, Z.; Huang, B.; Malinowski, P.; Wang, W.; Song, T.; Sanchez, J.; Yao, W.; Xiao, D.; Zhu, X.; May, A. F.; Wu, W.; Cobden, D. H.; Chu, J.-H.; Xu, X. Two-dimensional itinerant ferromagnetism in atomically thin Fe3GeTe2. *Nat. Mater.* **2018**, *17* (9), 778−782.

(27) Lee, J.-U.; Lee, S.; Ryoo, J. H.; Kang, S.; Kim, T. Y.; Kim, P.; Park, C.-H.; Park, J.-G.; Cheong, H. Ising-Type Magnetic Ordering in Atomically Thin FePS3. *Nano Lett.* **2016**, *16* (12), 7433−7438.

(28) Kim, K.; Lim, S. Y.; Lee, J.-U.; Lee, S.; Kim, T. Y.; Park, K.; Jeon, G. S.; Park, C.-H.; Park, J.-G.; Cheong, H. Suppression of magnetic ordering in XXZ-type antiferromagnetic monolayer NiPS3. *Nat. Commun.* **2019**, *10* (1), 345 DOI: 10.1038/s41467-018-08284-6.

(29) Gong, C.; Li, L.; Li, Z.; Ji, H.; Stern, A.; Xia, Y.; Cao, T.; Bao, W.; Wang, C.; Wang, Y.; Qiu, Z. Q.; Cava, R. J.; Louie, S. G.; Xia, J.; Zhang, X. Discovery of intrinsic ferromagnetism in two-dimensional van der Waals crystals. *Nature* **2017**, *546* (7657), 265−269.

(30) Jernberg, P.; Bjarman, S.; Wäppling, R. FePS3: A first-order phase transition in a "2D" Ising antiferromagnet. *J. Magn. Magn. Mater.* **1984**, *46* (1−2), 178−190.

(31) Little, A.; Lee, C.; John, C.; Doyle, S.; Maniv, E.; Nair, N. L.; Chen, W.; Rees, D.; Venderbos, J. W. F.; Fernandes, R. M.; Analytis, J. G.; Orenstein, J. Three-state nematicity in the triangular lattice antiferromagnet Fe1/3NbS2. *Nat. Mater.* **2020**, *19* (10), 1062−1067.

(32) Yang, K.; Kang, K.; Diao, Z.; Ramanathan, A.; Karigerasi, M. H.; Shoemaker, D. P.; Schleife, A.; Cahill, D. G. Magneto-optic response of the metallic antiferromagnet Fe2As to ultrafast temperature excursions. *Physical Review Materials* **2019**, *3* (12), 124408 DOI: 10.1103/PhysRevMaterials.3.124408.

(33) Malakhovskii, A. V.; Edelman, I. S. The role of the local magnetic mode in the optical absorption spectra of antiferromagnets. *Solid State Commun.* **1978**, *28* (6), 475−479.

(34) Kimel, A. V.; Astakhov, G. V.; Kirilyuk, A.; Schott, G. M.; Karczewski, G.; Ossau, W.; Schmidt, G.; Molenkamp, L. W.; Rasing, T. Observation of Giant Magnetic Linear Dichroism in(Ga,Mn)As. *Phys. Rev. Lett.* **2005**, *94* (22), 227203 DOI: 10.1103/PhysRevLett.94.227203.

(35) Momma, K.; Izumi, F. VESTA: a three-dimensional visualization system for electronic and structural analysis. *J. Appl. Crystallogr.* **2008**, *41* (3), 653−658.